Preprints.org

Article

Not peer-reviewed version

The Layered Oxyselenide BiCuSeO Has Garnered Significant Interest Because of Its Ability to Exhibit Low Thermal Conductivity and a High Seebeck Coefficient. This Study Involved the Preparation of Bi1−xNaxCuSeO1−xFx(x=0, 0.05, 0.10, 0.15, and 0.20) Ceramic

Zhenbing Pei , Guangqi Xiang , Xin Sun , Zhuang Fu , Yanxin Qiao , Lei Wang , Songtao Dong * , Jian Chen

Posted Date: 7 November 2023

doi: 10.20944/preprints202311.0427.v1

Keywords: high energy milling; bicuseo; thermoelectric performance; microstructure; double doping

Preprints.org is a free multidiscipline platform providing preprint service that is dedicated to making early versions of research outputs permanently available and citable. Preprints posted at Preprints.org appear in Web of Science, Crossref, Google Scholar, Scilit, Europe PMC.

Copyright: This is an open access article distributed under the Creative Commons Attribution License which permits unrestricted use, distribution, and reproduction in any medium, provided the original work is properly cited.

Preprints (www.preprints.org) | NOT PEER-REVIEWED | Posted: 7 November 2023 doi:10.20944/preprints202311.0427.v1

Disclaimer/Publisher's Note: The statements, opinions, and data contained in all publications are solely those of the individual author(s) and contributor(s) and not of MDPI and/or the editor(s). MDPI and/or the editor(s) disclaim responsibility for any injury to people or property resulting from any ideas, methods, instructions, or products referred to in the content.

Preprints.org

Article

Not peer-reviewed version

The Layered Oxyselenide BiCuSeO Has Garnered Significant Interest Because of Its Ability to Exhibit Low Thermal Conductivity and a High Seebeck Coefficient. This Study Involved the Preparation of Bi1−xNaxCuSeO1−xFx(x=0, 0.05, 0.10, 0.15, and 0.20) Ceramic

Zhenbing Pei , Guangqi Xiang , Xin Sun , Zhuang Fu , Yanxin Qiao , Lei Wang , Songtao Dong * , Jian Chen

Posted Date: 7 November 2023

doi: 10.20944/preprints202311.0427.v1

Keywords: high energy milling; bicuseo; thermoelectric performance; microstructure; double doping

Preprints.org is a free multidiscipline platform providing preprint service that is dedicated to making early versions of research outputs permanently available and citable. Preprints posted at Preprints.org appear in Web of Science, Crossref, Google Scholar, Scilit, Europe PMC.

Copyright: This is an open access article distributed under the Creative Commons Attribution License which permits unrestricted use, distribution, and reproduction in any medium, provided the original work is properly cited.

© 2023 by the author(s). Distributed under a Creative Commons CC BY license.

Preprints (www.preprints.org) | NOT PEER-REVIEWED | Posted: 7 November 2023 doi:10.20944/preprints202311.0427.v1

Disclaimer/Publisher's Note: The statements, opinions, and data contained in all publications are solely those of the individual author(s) and contributor(s) and not of MDPI and/or the editor(s). MDPI and/or the editor(s) disclaim responsibility for any injury to people or property resulting from any ideas, methods, instructions, or products referred to in the content.

Article

Effect of NaF Doping on the Microstructure and Thermoelectric Performance of BuCuSeO Ceramics

Zhenbing Pei [1], Guangqi Xiang [1], Xin Sun [1], Zhuang Fu [1], Yanxin Qiao [1], Lei Wang [1,*], Songtao Dong [1,] and Jian Chen [2]**

[1] School of Material Science and Engineering, Jiangsu University of Science and Technology, Zhenjiang, 212003, China

[2] Department of Chemistry, Western University, 1151 Richmond St., London, ON N6A 5B7, Canada

* Correspondence: information for L. Wang and S.−T. Dong can be obtained through the following email addresses: wangl_ray@just.edu.cn (L. Wang), stdong@just.edu.cn (S.−T. Dong).

Abstract: The layered oxyselenide BiCuSeO has garnered significant interest because of its ability to exhibit low thermal conductivity and a high Seebeck coefficient. This study involved the preparation of $Bi_{1-x}Na_xCuSeO_{1-x}F_x$(x=0, 0.05, 0.10, 0.15, and 0.20) ceramics through the processes of high energy ball milling and cold isostatic pressing. A systematic study was conducted to investigate the impact of co−doping Na/F on the thermoelectric performance of BiCuSeO ceramics. Replacing Bi^{3+} with Na^+ results in the introduction of a considerable amount of holes, leading to a notable enhancement in the electrical conductivity and power factor. The conductivity was significantly increased from 9.10 S cm^{-1} in the pure BiCuSeO to 94.5 S cm^{-1} in $Bi_{0.85}Na_{0.15}CuSeO_{0.85}F_{0.15}$ at 323 K. At 823 K, the power factor of the $Bi_{0.85}Na_{0.15}CuSeO_{0.85}F_{0.15}$ sample achieved 44.8×10^{-5} W/ m K^2. Moreover, the $Bi_{1-x}Na_xCuSeO_{1-x}F_x$ ceramics exhibit a minimum thermal conductivity of 0.43 W m^{-1} K^{-1}. As a result, the $Bi_{0.85}Na_{0.15}CuSeO_{0.85}F_{0.15}$ sample achieves a maximum ZT value of 0.78, which is 7.09 times greater than that of the pure BiCuSeO sample (0.11) .

Keywords: high energy milling; BiCuSeO; thermoelectric performance; microstructure; double doping

1. Introduction

The issues of environmental pollution and energy crisis are escalating at an alarming rate. Currently, in the conventional procedure of utilizing fossil energy, only a relatively minor portion of the mineral energy is transformed and employed, with the majority of the remaining energy being dissipated as heat [1]. Extensive studies have been conducted by scientists to discover renewable and eco−friendly energy sources while enhancing energy efficiency. Carrier and phonon transmission characteristics within solid materials are utilized by thermoelectric materials to achieve the direct conversion between electric energy and heat energy, emerging as a novel environmentally−friendly energy material [2]. The dimensionless optimal values determine the thermoelectric characteristics of materials, which can be obtained using the equation by $ZT = S^2\sigma T/\kappa$. Here, S, σ, T, and κ represent the Seebeck coefficient, electrical conductivity, absolute temperature, and thermal conductivity, respectively[3−5]. Nonetheless, the interdependence of S, ϱ, and κ poses a barrier to the collaborative enhancement of thermoelectric performance, presenting a significant obstacle in achieving simultaneous optimization of multiple parameters [6,7]. The concept of phonon glass electron crystals offers a potential solution to this puzzle [8]. The low thermal conductivity and high Seebeck coefficient of the BiCuSeO system have garnered significant interest [9−11]. Figure 1a illustrates that BiCuSeO has a layered structure of the ZrCuSiAs type and is classified under the P4/nmm space group. The crystal structure consists of a stack of alternating layers along the C−axis direction. These layers include an insulating layer $(Bi_2O_2)^{2+}$ and a conducting layer $(Cu_2Se_2)^{2-}$. The Bi_2O_2 layer serves as a charge storage layer, composed of a slightly deformed Bi_4O octahedron with shared Bi−Bi edges. On the other hand, the Cu_2Se_2 layer acts as a transport surface for carrier transport, composed of slightly deformed $CuSe_4$ tetrahedra with shared Se−Se sides [12−14]. Furthermore, the feeble chemical

© 2023 by the author(s). Distributed under a Creative Commons CC BY license.

Preprints (www.preprints.org) | NOT PEER-REVIEWED | Posted: 7 November 2023 doi:10.20944/preprints202311.0427.v1

linkage amidst the two layers and the junction connecting them enhance phonon scattering, leading to an extremely low thermal conductivity (0.40 $Wm^{-1}K^{-1}$ at 923 K) [9].

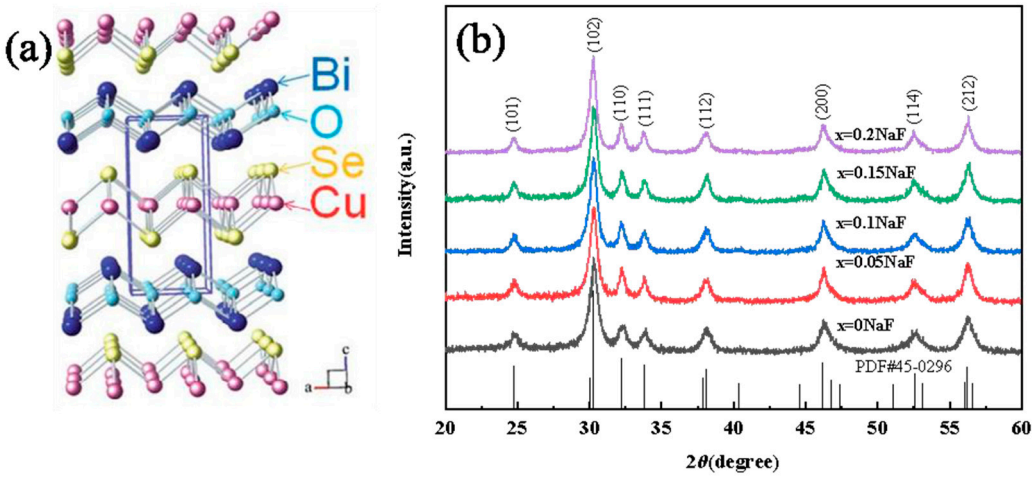

Figure 1. (a) Schematic diagram of the crystal structure of BiCuSeO; (b) XRD pattern of $Bi_{1-x}Na_xCuSeO_{1-x}F_x$(x = 0, 0.05, 0.10, 0.15, and 0.20) ceramics.

Nonetheless, BiCuSeO exhibits a significantly limited conductivity as a result of its low hole concentration, thereby impeding the attainment of a high ZT value. In order to enhance the conductivity of BiCuSeO, the researchers enhanced the material's conductivity through element doping, optimized the carrier concentration by adjusting the band gap, and increased the carrier mobility through texturization [18,19]. Doping monovalent elements (Na^+, K^+, Ag^+, etc.) or bivalent elements (Mg^{2+}, Ca^{2+}, Ba^{2+}, Pb^{2+}, etc.) at the Bi site or by increasing the concentration of hole carriers through Bi, Cu, O vacancies and ball−milling is used to improve the thermoelectric performance of BiCuSeO [10−13,15−17]. Furthermore, the technique of dual doping is another efficient approach for enhancing the thermoelectric performance of materials. Sun et al enhanced the thermoelectric characteristics of BiCuSeO by introducing Zn into the Bi position and S into the O position, resulting in a ZT value of 0.68 at 750 K [20]. Kuang−kun Ren et al introduced dopants of Pb and Te into the Bi and Se positions, respectively. The substitution of Te at Se sites significantly decreased the extent of chemical bonding and the mass of effective carriers. Consequently, this weakened the coupling between carriers and phonons, enhancing carrier mobility and resulting in high conductivity [21]. By employing mechanical alloying, the BiCuSeO system achieved a ZT value of 1.08 through the introduction of Pb and Ni elements into the Bi and Cu sites [18]. The replacement of Bi elements with Pb and In elements resulted in the ZT value of the BiCuSeO system reaching 1.23 [22]. Liu et al. reported that the addition of Pb and Ca elements into the Bi site of BiCuSeO not only improved the conductivity and thermal conductivity, but also enhanced the effective mass of carriers, thereby maintaining a high Seebeck coefficient for the material. Consequently, the doped BiCuSeO achieved a ZT value of 1.5 [23], which stands as the highest value within the present system.

The above results show that co−doping of elements can enhance the thermoelectric performance of BiCuSeO. Although there have been numerous reports on the Bi, Cu, and Se dopants of BiCuSeO, there is comparatively less information available on the O−dopants. Furthermore, studies [10] and [24] have indicated that the thermoelectric performance of the BiCuSeO system can be enhanced through O−site doping of F and S elements. The majority of the materials are synthesized through the sintering technique of solid state reaction. The drawback of this approach is the lengthy requirement for calcination of the raw materials, whereas the high−energy ball milling technique enables rapid synthesis of the raw materials. Considering this, the rapid synthesis of Na and F co−doped BiCuSeO ceramic samples was achieved using the high energy ball milling technique. A systematic study was conducted on the impact of combining sodium in the bismuth position and fluorine in the oxygen position on the microstructure and thermoelectric performance of BiCuSeO.

Preprints (www.preprints.org) | NOT PEER-REVIEWED | Posted: 7 November 2023 doi:10.20944/preprints202311.0427.v1

2. Experimental

2.1. Synthesis of starting material

$Bi_{1-x}Na_xCuSeO_{1-x}F_x$(x=0, 0.05, 0.10, 0.15, and 0.20) ceramics were fabricated through the processes of high energy ball milling and cold isostatic pressing. Firstly, according to the chemical formula of $Bi_{1-x}Na_xCuSeO_{1-x}F_x$, the mass of the raw material was calculated according to 0.045mol. Bi_2O_3 with purity of 99.999% and Bi, Cu, Se and NaF with purity of 99.99% were selected, where x= 0,0.05, 0.10, 0.15 and 0.20. Secondly, the raw material powder of $Bi_{1-x}Na_xCuSeO_{1-x}F_x$ was measured and placed into a ball mill tank of high energy planetary ball mill for milling. The ball mill tank and the ball used was a 500 ml cemented carbide ball grinding tank and 10 mm diameter cemented carbide ball, respectively. The ratio of ball and material was 30:1, and the milling speed was 560 rpm. The milling process was lasted for 2 hours. To prevent the high temperature in the ball milling process and produce side reactions, the cycle of '10 minutes ball milling +3 minutes cooling was implemented during the process. After undergoing ball milling, the powdered sample was inserted into a lengthy rubber balloon, molded into 10 mm and 15 mm diameters, and subsequently subjected to a 20−minute cold isostatic pressing process at a pressure of 300 MPa. Next, the acquired rod sample was hermetically sealed in a quartz tube (vacuum ~10^{-3} pa), gradually heated to 450℃ at a rate of 5 ℃/min, and subjected to a 2−hour calcination process in a Muffle furnace. Employing low temperature sintering helps to suppress the enlargement of the ceramic sample's grains. Finally, the sintered sample is cut into sizes of 15 mm × 3 mm × 3 mm and ⌀12.5 mm × 2 mm for thermoelectric performance testing.

2.2. Structure and transport performance characterization

X−ray diffractometer (XRD, Bruker D8 Advance) was used to conduct on phase analysis of $Bi_{1-x}Na_xCuSeO_{1-x}F_x$(x=0, 0.05, 0.10, 0.15, and 0.20) ceramics. XRD testing was conducted using the Cu K_α line, with a scanning range from 20° to 60°. The test was performed at 40 kV and 40 mA at a scanning speed of 4°/min. The fracture morphology of ceramics was analyzed by field emission scanning electron microscopy (FESEM; Merlin Compact, Carl Zeiss, Germany). X−ray photoelectron spectroscopy (XPS) was used to examine the valence states of the samples. The Seebeck coefficient and resistivity were simultaneously measured on a ZEM−3 thermoelectric performance tester using standard DC four−probe techniques. The thermal conductivity (κ) was calculated by $\kappa = \varrho DCp$, where ϱ is the volumetric density determined by the Archimedes method, D is the thermal diffusivity measured using a laser flash apparatus (LFA 457, Netzsch), and Cp is the specific heat obtained using a differential scanning calorimetry thermal analyzer (DSC 8000, PerkinElmer).The Hall coefficient (R_H) was obtained by the Physical Property Measurement System (PPMS, Quantum Corporation). The carrier concentration was extracted by means of

single−electron approximation ($R_H = \frac{1}{n \cdot e}$, R_H, n, and e are Hall coefficient, carrier concentration, and electron charge, respectively).

3. Results and discussion

The XRD patterns of $Bi_{1-x}Na_xCuSeO_{1-x}F_x$(x=0, 0.05, 0.10, 0.15, and 0.20) ceramics is depicted in Figure 1b. Compared to the standard card of BiCuSeO (PDF#45−0296), the diffraction peak position of the $Bi_{1-x}Na_xCuSeO_{1-x}F_x$ was consistent with that of the standard card. The results show that the synthesized $Bi_{1-x}Na_xCuSeO_{1-x}F_x$ ceramics is a single phase. As the NaF doping amount increased, the XRD peak of $Bi_{1-x}Na_xCuSeO_{1-x}F_x$ ceramics experienced a slight rightward shift. This shift occurred due to the slightly smaller ionic radius of Na^+ (0.102 nm) compared to Bi^{3+} (0.103 nm), and the smaller ionic radius of F^-(0.133 nm) compared to O^{2-} (0.140 nm). This makes the crystal plane spacing smaller. The crystal face spacing and the lattice constants are were calculated using the Bragg Eqs. (1) and (2):

$$\lambda = 2d_{hkl}sin\theta_{hkl} \quad (1)$$

Preprints (www.preprints.org) | NOT PEER-REVIEWED | Posted: 7 November 2023 doi:10.20944/preprints202311.0427.v1

$$\frac{1}{d^2} = \frac{h^2 + k^2}{a^2} + \frac{l^2}{c^2} \quad (2)$$

where d, a, and c represents the crystal plane spacing, and lattice parameters, correspondingly. Table 1 displays the lattice constants a and c of $Bi_{1-x}Na_xCuSeO_{1-x}F_x$ (x=0, 0.05, 0.10, 0.15, and 0.20) ceramics. The crystal face spacing of $Bi_{1-x}Na_xCuSeO_{1-x}F_x$ ceramic sample was calculated by the equation (2), and it was found that the change of crystal face spacing was very small. Therefore, the diffraction peak of $Bi_{1-x}Na_xCuSeO_{1-x}F_x$ ceramics did not appear obvious deviation. Table 1 shows the calculation of the grain size for $Bi_{1-x}Na_xCuSeO_{1-x}F_x$ ceramics using the Debye–Scherrer formula $Dc = 0.89\lambda/(B\cos\theta)$, where B represents the half–peak width and θ signifies the Bragg diffraction Angle. The results show that the average grain sizes of $Bi_{1-x}Na_xCuSeO_{1-x}F_x$(x=0, 0.05, 0.10, 0.15, and 0.20) ceramics are 1.92 μm, 1.63 μm, 1.66 μm, 1.68 μm, and 1.72 μm, correspondingly. Following the addition of NaF, the average grain size of the $Bi_{1-x}Na_xCuSeO_{1-x}F_x$ samples is marginally reduced compared to the pure BiCuSeO sample. The fracture morphology of $Bi_{1-x}Na_xCuSeO_{1-x}F_x$(x=0, 0.05, 0.10, 0.15, and 0.20) ceramics is shown in Figure 2, illustrating the layered structures. According to Figure 2, the average grain size of $Bi_{1-x}Na_xCuSeO_{1-x}F_x$ samples exhibited a pattern of initial decrease and subsequent increase as the NaF doping amount increased, aligning with the results obtained from the Scherrer formula calculations.

Table 1. Lattice parameters and grain sizes of $Bi_{1-x}Na_xCuSeO_{1-x}F_x$(x = 0, 0.05, 0.10, 0.15, and 0.20).

Samples	a(Å)	c(Å)	grain size (μm)
x = 0	3.93908	8.90968	1.92
x = 0.05	3.92563	8.92035	1.63
x = 0.1	3.91786	8.92214	1.66
x = 0.15	3.91661	8.93309	1.68
x = 0.2	3.92251	8.93120	1.72

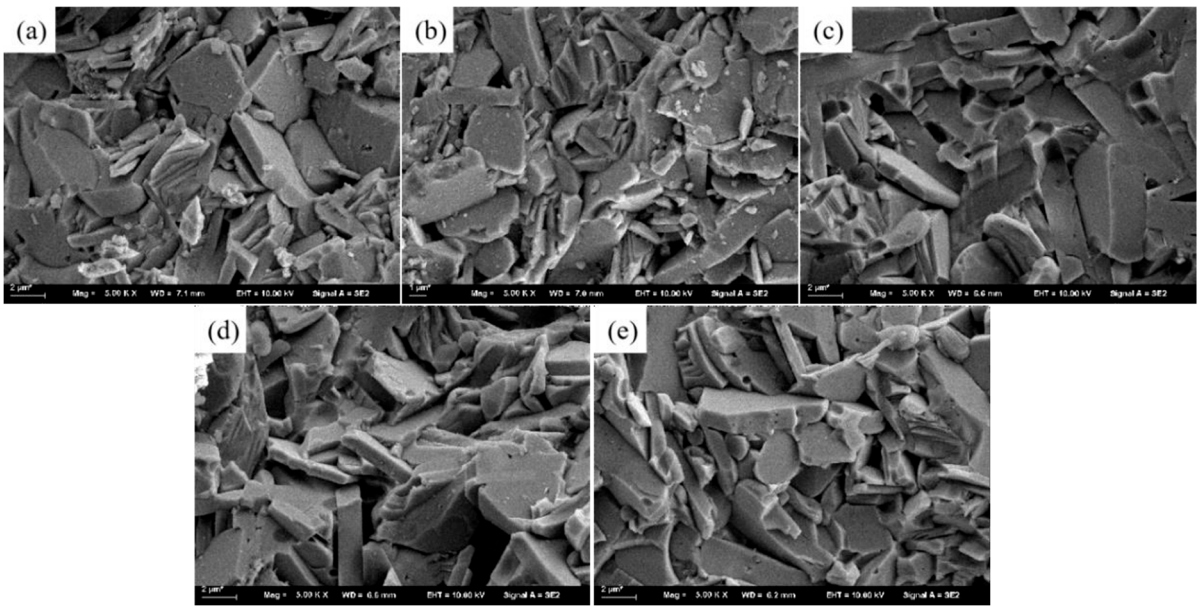

Figure 2. Fracture morphology of $Bi_{1-x}Na_xCuSeO_{1-x}F_x$(x = 0, 0.05, 0.10, 0.15, and 0.20) ceramics.

XPS determination was conducted on the $Bi_{1-x}Na_xCuSeO_{1-x}F_x$ (x = 0,0.05, 0.10, 0.15, and 0.20) ceramics to ascertain the valence states of each element. Figure 3a shows the full spectrum of XPS of $Bi_{1-x}Na_xCuSeO_{1-x}F_x$ (x=0, 0.15) ceramic sample. It can be seen from the full spectrum that the undoped sample contains Bi, Cu, Se and O elements, while the doped NaF sample contains Bi, Cu, Se, O, Na and F elements. Combined with XRD results, it is possible to verify the successful integration of Na and F elements into the BiCuSeO system. The XPS high–resolution spectra of

Preprints (www.preprints.org) | NOT PEER-REVIEWED | Posted: 7 November 2023 doi:10.20944/preprints202311.0427.v1

Bismuth (Bi), Copper (Cu), Selenium (Se), Oxygen (O), and Sodium (Na) in the samples of $Bi_{1-x}Na_xCuSeO_{1-x}F_x$ (x=0, 0.15) samples are displayed in Fgure 3(a)−(f). The high−resolution spectra of Bi 4f in Figure 3b exhibits two spin−orbit peaks, which correspond to the spin−orbit peak of Bi $4f_{7/2}$ and the spin−orbit peak of Bi $4f_{5/2}$, respectively. The two distinctive peaks can be found at 158.28 eV and 163.58 eV correspondingly, with a disparity of 5.3 eV, suggesting the presence of Bi atoms in the Bi^{3+} state [17,25,26]. As shown in the Figure 3c, the 2p orbits of Cu elements in the pure BiCuSeO sample split into two distinct peaks, namely the spin−orbit peak of Cu $2p_{3/2}$ at 931.68 eV and the spin−orbit peak of Cu $2p_{1/2}$ at 951.58 eV. These peaks exhibit a difference of 19.9 eV, indicating the presence of Cu+ ions in the sample. The spin−orbit splitting of Cu 2p in the $Bi_{0.85}Na_{0.15}CuSeO_{0.85}F_{0.15}$ sample is divided into four peaks. According to the results, Cu^{2+} is observed in the $Bi_{0.85}Na_{0.15}CuSeO_{0.85}F_{0.15}$, which aligns with the outcomes documented in the literature [26]. Figure 3d shows the Se 3d high−resolution spectrum. The spin−orbit splitting is quite intricate, with the spin−orbit peaks of Se $3d_{5/2}$ located at 53.48 eV and 54.88 eV, respectively. The spin−orbit peaks of Se $3d_{3/2}$ were found at 54.28 eV and 55.48 eV, correspondingly. The presence of Se atoms in the form of Se^{2-} is indicated by the low binding energy of the Se $3d_{5/2}$ and Se $3d_{3/2}$ spin−orbit peaks, while the interaction between the layers of Se is indicated by the high binding energy of the spin−orbit peaks, which aligns with the results documented in the literature [26]. The high−resolution spectrum of O 1s in Figure 3e reveals two spin−orbit peaks. The peak at 529.4 eV represents lattice oxygen, whereas the high binding energy peak signifies oxygen vacancy. To ascertain the alteration in oxygen content for the two types, the ratio of the two peaks' areas was employed. The area ratio of lattice oxygen to oxygen vacancy in the BiCuSeO sample is 0.2, while the area ratio of lattice oxygen to oxygen vacancy in the $Bi_{0.85}Na_{0.15}CuSeO_{0.85}F_{0.15}$ sample is 0.09. The results indicate that the doping of NaF increases the lattice defect in $Bi_{1-x}Na_xCuSeO_{1-x}F_x$ sample, which aligns with the results reported documented in the literature [27,28]. Figure 3f shows the high−resolution spectrum of Na 1s in $Bi_{0.85}Na_{0.15}CuSeO_{0.85}F_{0.15}$ samples. The Na 1s orbital exhibits a solitary peak, indicating that Na exists with a +1 valence, which aligns with the results documented in the literature [29]. The 1s spin-orbit peak of F in Figure 3g, indicates the presence of F^- in a manner consistent with the results reported in the literature[30].

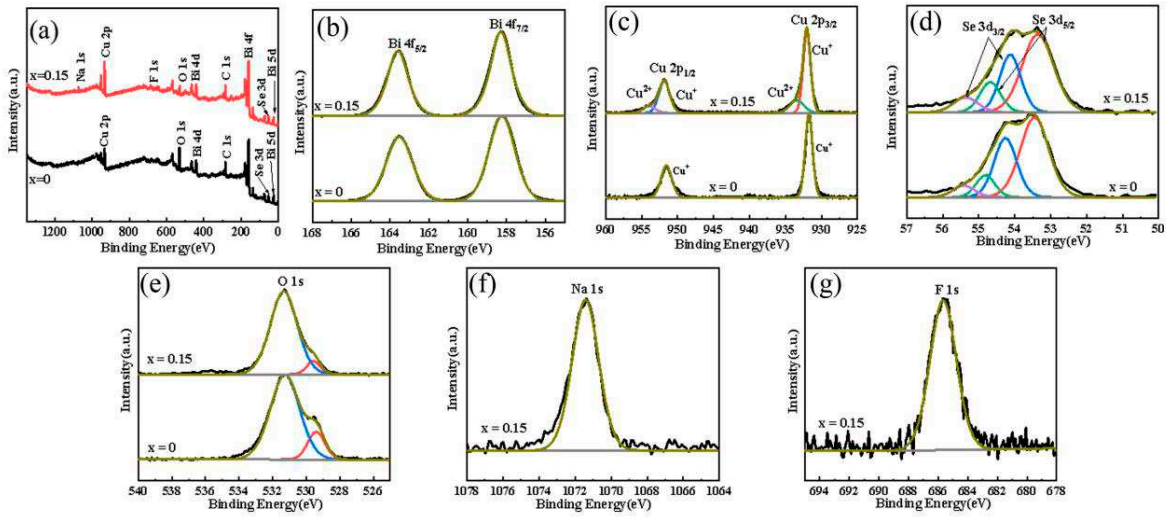

Figure 3. (a) Full spectrum of $Bi_{1-x}Na_xCuSeO_{1-x}F_x$ (x=0, 0.15) ceramics, (b) Bi 4f, (c) Cu 2p, (d) Se 3d, (e) O 1s, (f) Na 1s, (g) F 1s high−resolution spectrum.

The temperature−dependent electrical conductivity (σ) of the $Bi_{1-x}Na_xCuSeO_{1-x}F_x$ (x = 0, 0.05, 0.10, 0.15, and 0.20) ceramics is shown in Figure 4a. For the pure BiCuSeO sample, the conductivity is very low throughout the test temperature range, and is significantly improved after doping. The σ of $Bi_{1-x}Na_xCuSeO_{1-x}F_x$ ceramics increases as the NaF doping increases in the whole temperature range. At 323 K, the conductivity increases from 9.10 S cm^{-1} (BiCuSeO) to 94.50 S cm^{-1}

Preprints (www.preprints.org) | NOT PEER-REVIEWED | Posted: 7 November 2023 doi:10.20944/preprints202311.0427.v1

($Bi_{0.80}Na_{0.20}CuSeO_{0.80}F_{0.20}$), resulting in a significant increase of 900%. The rise in the carrier concentration of the system is the primary cause for the enhanced conductivity of $Bi_{1-x}Na_xCuSeO_{1-x}F_x$ (x = 0, 0.05, 0.10, 0.15, and 0.20) ceramics. The relationship between conductivity σ and carrier concentration and mobility can be expressed as $\sigma=enu$, where e represents the electron charge, n denotes the carrier concentration, and μ represents the carrier mobility. The carrier concentration is determined using the expression $n=1/eR_H$. Table 2 demonstrates the carrier concentration and mobility of $Bi_{1-x}Na_xCuSeO_{1-x}F_x$ (x = 0, 0.05, 0.10, 0.15, and 0.20) ceramics. Upon the addition of NaF, the electrical conductivity σ initially declines and subsequently rises as the testing temperature increases, reaching an inflection point at 523 K. Within the temperature range from 323 K to 523 K, the conductivity of the doped ceramics diminishes with rising temperature, exhibiting degenerate semiconductor characteristics. As the temperature exceeds 523 K, the sample's conductivity rises in proportion to the temperature increase. The sample displays semiconductor performance that are not degenerate due to its intrinsic excitation. The conductivity of $Bi_{0.80}Na_{0.20}CuSeO_{0.80}F_{0.20}$ reaches a maximum of 108.6 S cm^{-1} at 823 K.

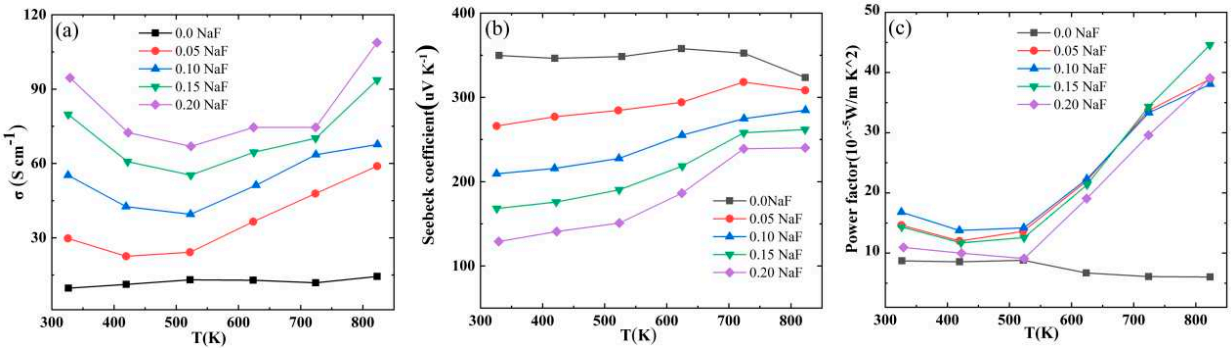

Figure 4. Temperature-dependent (a) electrical conductivity, (b) Seebeck coefficient S and (c) PF of $Bi_{1-x}Na_xCuSeO_{1-x}F_x$ (x = 0, 0.05, 0.10, 0.15, and 0.20) ceramics.

Table 2. Carrier concentration, mobility, effective mass, and density of $Bi_{1-x}Na_xCuSeO_{1-x}F_x$ (x = 0, 0.05, 0.10, 0.15, and 0.20) ceramics at room temperature.

Samples	n(10^{18} cm^{-3})	μ (cm^2 V^{-1} S^{-1})	m* (m_0)	ϱ (g/cm^3)
x = 0	0.99	6.109	2.0940	7.517
x = 0.05	7.54	2.466	4.1580	7.495
x = 0.1	10.3	3.352	3.1936	7.473
x = 0.15	51.5	0.969	6.5043	7.444
x = 0.2	57.8	1.022	4.8277	7.367

Figure 4b shows temperature−dependent S of $Bi_{1-x}Na_xCuSeO_{1-x}F_x$ (x=0, 0.05, 0.10, 0.15, and 0.20) ceramics. The signs for all Seebeck coefficients are positive, indicating that the $Bi_{1-x}Na_xCuSeO_{1-x}F_x$ ceramic functions as a P-type semiconductor with predominantly hole charge carriers. The Seebeck coefficient of BiCuSeO exhibits a value of 349 uV K^{-1} at 323 K, while it shows a value of 324 uV K^{-1} at 823 K.The Seebeck coefficient of $Bi_{1-x}Na_xCuSeO_{1-x}F_x$ samples decreases as NaF doping content increases at 300 K. In the case of degenerate semiconductors, if we assume a parabolic band structure and use the phonon scattering approximation, the Pisarenko relationship can provide a rough representation of S [31,32].

$$S = \frac{8\pi^2 {k_B}^2 T}{3eh^2} m^* \left(\frac{\pi}{3n}\right)^{2/3} \quad (3)$$

The Seebeck coefficient (S), Boltzmann constant (k_B), absolute temperature (T), carrier charge (e), reduced Planck constant (h), carrier effective mass (m^*), and carrier concentration (n) are all related in this equation. Formula (3) reveals that the Seebeck coefficient varies inversely with the carrier

Preprints (www.preprints.org) | NOT PEER-REVIEWED | Posted: 7 November 2023 doi:10.20944/preprints202311.0427.v1

concentration and directly with the effective mass. The effective mass m* is calculated by formula (3), as shown in Table 2. The effective mass m* increases as the NaF doping content increases, going from 2.094 m_0 in the pure sample to 6.5043 m_0 in the $Bi_{0.85}Na_{0.15}CuSeO_{0.85}F_{0.15}$ sample. The results indicate that the decline in Seebeck coefficient of $Bi_{1-x}Na_xCuSeO_{1-x}F_x$ ceramics primarily arises from the rise in increase of carrier concentration within the system.

The power factor of $Bi_{1-x}Na_xCuSeO_{1-x}F_x$ (x = 0, 0.05, 0.10, 0.15, and 0.20) ceramics is determined by the formula $PF=S^2\sigma$. The temperature dependent curves for the power factor are shown in Figure 4c. The PF of all doped samples is higher than that of pure BiCuSeO throughout the entire temperature range due to a substantial conductivity increase. At room temperature, the $Bi_{0.90}Na_{0.10}CuSeO_{0.90}F_{0.10}$ samples have the highest power factor, reaching 16.7 × 10^{-5} W/m K^{-2}. As the temperature increases, the power factor of $Bi_{0.85}Na_{0.15}CuSeO_{0.85}F_{0.15}$ samples gradually surpasses that of $Bi_{0.90}Na_{0.10}CuSeO_{0.90}F_{0.10}$ samples. At 823 K, the $Bi_{0.85}Na_{0.15}CuSeO_{0.85}F_{0.15}$ sample exhibits a maximum power factor of 44.8 × 10^{-5} W/m K^2, which is approximately 7.11 times higher than that of the pure BiCuSeO sample (6.3×10^{-5} W/mK^2).

Figure 5a shows thermal conductivity (κ) as a function of temperature for $Bi_{1-x}Na_xCuSeO_{1-x}F_x$ (x = 0, 0.05, 0.10, 0.15, and 0.20) ceramics. The thermal conductivity κ of BiCuSeO significatly decreases from 0.98 Wm^{-1} K^{-1} at 323 K to 0.43 Wm^{-1} K^{-1} at 823 K, while the thermal conductivity remained virtually unchanged even after the introduction of NaF doping. Typically, the total thermal conductivity consists of the electron thermal conductivity κ_e and the lattice thermal conductivity κ_l. The electron thermal conductivity is usually calculated by Wiedemane−Franz relationship ($\kappa_e = L\sigma T$) , where σ is the electrical conductivity, T is the absolute temperature, and L is the Lorentz constant which can be calculated by the formula $L = 1.5 + exp\left(\frac{-|S|}{116}\right)$. Lorentz constant L is calculated using Sommerfeld value L_0= 2.44×10^{-8} W Ω K^{-2}. Figure 5b displays the temperature dependence of the electron thermal conductance κ_e of $Bi_{1-x}Na_xCuSeO_{1-x}F_x$ (x = 0, 0.05, 0.10, 0.15, and 0.20) ceramics. The figure illustrates that the electron thermal conductivity of $Bi_{1-x}Na_xCuSeO_{1-x}F_x$ ceramics exhibits a rising pattern as the doping level increases. The primary reason for this is primarily the rise in electrical conductance. At 823 K, the maximum electron thermal conductivity of $Bi_{0.8}Na_{0.2}CuSeO_{0.8}F_{0.2}$ ceramics reaches 0.219 W m^{-1} K^{-1}. The results indicate that the lattice thermal conductivity is dominant in the BiCuSeO system.

The temperature-dependent lattice thermal conductivity of $Bi_{1-x}Na_xCuSeO_{1-x}F_x$ (x = 0, 0.05, 0.10, 0.15, and 0.20) ceramics is illustrated in Figure 5c. The lattice thermal conductivity of $Bi_{1-x}Na_xCuSeO_{1-x}F_x$ samples declines as the temperature rises. This was primarily due to the intensification of lattice vibration and the enhanced scattering ability of phonons, resulting in a decrease in lattice thermal conductivity as temperature increases. Compared to the pure BiCuSeO sample, the lattice thermal conductivity of $Bi_{1-x}Na_xCuSeO_{1-x}F_x$ ceramics decreases, primarily due to the reduction in grain size caused by NaF doping. Table 1 displays that the grain sizes of $Bi_{1-x}Na_xCuSeO_{1-x}F_x$ (x = 0, 0.05, 0.10, 0.15, and 0.20) ceramics are 1.92 μm, 1.63 μm, 1.66 μm, 1.68 μm, and 1.72 μm, respectively. The grain sizes of the doped samples are smaller compared to the pure BiCuSeO sample, leading to an improved ability for scattering phonons. Hence, the lattice thermal conductivity of $Bi_{1-x}Na_xCuSeO_{1-x}F_x$ ceramics doped with NaF decreases as the doping amount increases.

The ZT as a function of temperature for $Bi_{1-x}Na_xCuSeO_{1-x}F_x$ (x = 0, 0.05, 0.10, 0.15, and 0.20) ceramics is illustrated in figure 5(d). The ZT value of $Bi_{1-x}Na_xCuSeO_{1-x}F_x$ samples is primarily determined by its electrical conductivity due to the insignificant variation in thermal conductivity.The figure illustrates that the ZT value of all samples exhibits an increasing trend with the increase of test temperature. At 823 K, and $Bi_{0.85}Na_{0.15}CuSeO_{0.85}F_{0.15}$ achieves a peak value of 0.78, which is 7.09 times greater than that of pure BiCuSeO. The results indicate that the addition of NaF can greatly enhance the thermoelectric performance of BiCuSeO.

Preprints (www.preprints.org) | NOT PEER-REVIEWED | Posted: 7 November 2023 doi:10.20944/preprints202311.0427.v1

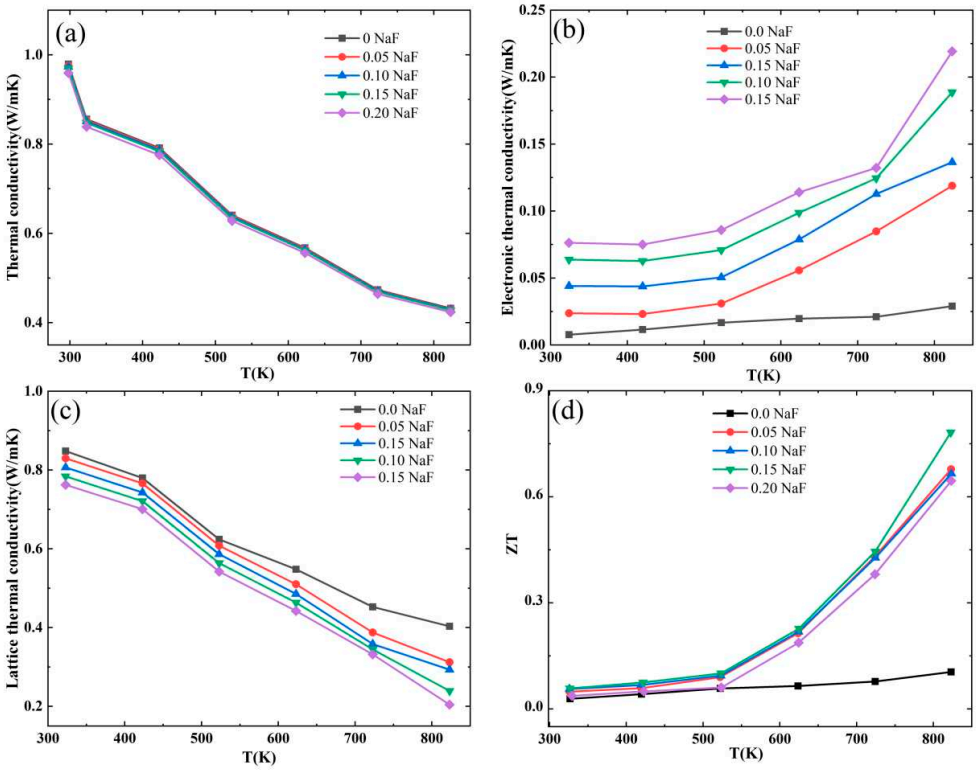

Figure 5. Temperature dependence of the (a) total thermal conductivity κ, (b) electronic thermal conductivity κ_e (c) lattice thermal conductivity κ, (d) ZT value of $Bi_{1-x}Na_xCuSeO_{1-x}F_x$ (x = 0, 0.05, 0.10, 0.15, and 0.20) ceramics.

4. Conclusions

In this work, NaF doped BiCuSeO was successfully synthesized through the combination of high energy ball milling and cold isostatic pressing. The addition of both Na and F elements resulted in a decrease in the grain size of $Bi_{1-x}Na_xCuSeO_{1-x}F_x$ samples, an increase in the carrier concentration, and subsequently enhances the electrical conductivity. The power factor of the pure sample increases from 6.3×10^{-5} W/m K^2 to 44.8×10^{-5} W/mK^2 in the $Bi_{0.85}Na_{0.15}CuSeO_{0.85}F_{0.15}$ sample at 823 K. The smaller grain size of the doped samples improves the system's ability to scatter phonons, consequently decreasing the lattice thermal conductivity. The $Bi_{0.85}Na_{0.15}CuSeO_{0.85}F_{0.15}$ sample achieves a maximum ZT value of 0.78 at 823 K, exhibiting a 7.09-fold increase (0.11) compared to the original BiCuSeO sample. The above results indicate that co−doping is asuccessful approach for enhancing the thermoelectric performance of the materials.

Author Contributions: Conceptualization and data curation, Z.-B. P.; methodology and formal analysis, Z.F.; investigation, M.-C.Y.; investigation, L. Z.; writing—original draft preparation, S.-T. D.; writing—review and editing, L.W. All authors have read and agreed to the published version of the manuscript.

Acknowledgments: The authors express gratitude for the financial assistance provided by the National Natural Science Foundation of China (51702132), and Songtao Dong acknowledges the open project of National Laboratory of Solid-State Microstructures, Nanjing University.

Conflicts of Interest: The authors declare no conflict of interest.

References

1. X. F. Zheng, C. X. Liu, Y. Y. Yan, et al. A review of thermoelectrics research–Recent developments and potentials for sustainable and renewable energy applications. Renewable and Sustainable Energy Reviews, 2014, 32(32): 486−503.
2. X. L. Shi, J. Zou, Z. G. Chen, Advanced Thermoelectric Design: From Materials and Structures to Devices, Chemical Reviews, 2020, 120: 7399–7515.

Preprints (www.preprints.org) | NOT PEER-REVIEWED | Posted: 7 November 2023 doi:10.20944/preprints202311.0427.v1

3. Song−Tao Dong, Miao−Cheng Yu, Zhuang Fu, Yang−Yang Lv, Shu−Hua Yao, Y.B. Chen, High thermoelectric performance of NaF−doped Bi2Ca2Co2Oy ceramic samples,Journal of Materials Research and Technology, 2022, 17, 1598−1604.
4. Zhuang Fu, Jia−Ling Jiang, Song−Tao Dong, Miao−Cheng Yu, Lijun Zhao, Lei Wang, Shu−Hua Yao, Effects of Zr substitution on structure and thermoelectric performance of Bi2O2Se, Journal of Materials Research and Technology,2022, 21, 640−647.
5. Jia-Ling Jiang, Song-Tao Dong , Zhuang Fu, Miao-Cheng Yu, Lijun Zhao and Lei Wang, Effect of Ta Doping on the Microstructure and Thermoelectric performance of Bi2O2Se, Metals 2022, 12, 1881.
6. T. Mori, Novel principles and nanostructuring methods for enhanced thermoelectrics, Small, 2017, 13: 1702013.
7. J. He, T. M. Tritt, Advances in thermoelectric materials research: looking back and moving forward, Science, 2017,357:eaak9997.
8. G. A. Slack, and D. Rowe, CRC handbook of thermoelectrics. 1995, CRC press Boca Raton, F L.
9. Liu Y, Zhao L D, Liu Y, et al. Remarkable enhancement in thermoelectric performance of BiCuSeO by Cu deficiencies. J Am Chem Soc, 2011, 133(50): 20112−5.
10. Li F, Wei T R, Kang F Y, et al. Enhanced thermoelectric performance of Ca−doped BiCuSeO in a wide temperature range. Journal of Materials Chemistry A, 2013, 1(38): 11942−11949.
11. Ren G K, Lan J L, Butt S, et al. Enhanced thermoelectric performance in Pb−doped BiCuSeO oxyselenides prepared by ultrafast synthesis. RSC Advances, 2015, 5(85): 69878−69885.
12. Li J, Sui J, Barreteau C, et al. Thermoelectric performance of Mg doped p−type BiCuSeO oxyselenides. Journal of Alloys and Compounds, 2013, 551: 649−653.
13. Li J S, Pei J, Barreteau Y, et al. A high thermoelectric figure of merit ZT> 1 in Ba heavily doped BiCuSeO oxyselenides. Energy Environ. Sci, 2012, 5(9): 8543−8547.
14. Li J, Sui J, Pei Y L, et al. The roles of Na doping in BiCuSeO oxyselenides as a thermoelectric material. Journal of Materials Chemistry A, 2014, 2(14): 4903−4906.
15. Zhao L D, Berardan D, Pei Y L, et al. Bi1−xSrxCuSeO oxyselenides as promising thermoelectricmaterials. Applied Physics Letters, 2010, 97(9): 092118.
16. Lan J L, Ma W, Deng C, et al. High thermoelectric performance of Bi1−xKxCuSeO prepared by combustion synthesis. Journal of Materials Science, 2017, 52(19): 11569−11579.
17. Liu Y C, Lan J L, Zhan B, et al. Thermoelectric performance of Pb−doped BiCuSeO ceramics. Journal of the American Ceramic Society, 2013, 96(9): 2710−2713.
18. Feng B, Li G, Pan Z, et al. Enhanced thermoelectric performance in BiCuSeO ceramics by Pb/Ni dual doping and 3D modulation doping. Journal of Solid State Chemistry, 2019, 271: 1−7.
19. Park K, Kim D H, Hong H Y, et al. Influence of Ba2+ doping on the thermoelectric performance of BiCuSeO fabricated by spark plasma sintering. Ceramics International, 2019, 45(7): 9604−9610.
20. Sun Y, Zhang C, Cao C, et al. Enhanced thermoelectric performance in BiCuSeO oxyselenides via Zn and S dual−site substitution. Journal of Electronic Materials, 2017, 46(10): 5909−5915.
21. Ren G K, Wang S Y, Zhu Y C, et al. Enhancing thermoelectric performance in hierarchically structured BiCuSeO by increasing bond covalency and weakening carrier–phonon coupling. Energy & Environmental Science, 2017, 10(7): 1590−1599.
22. Xiaolong Liang, Rui Xu, Mengruizhe Kong, Han Wan, Wei Bai, Deming Dong, Qizhu Li, Huihong Xu, Zhou Li, Binghui Ge, Jiming Song, Chong Xiao,Raising the thermoelectric performance in Pb/In−codoped BiCuSeO by alleviating the contradiction between carrier mobility and lattice thermal conductivity, Materials Today Physics, 2023, 34,101084,
23. Liu Y, Zhao L D, Zhu Y, et al. Synergistically optimizing electrical and thermal transport performance of BiCuSeO via a dual−doping approach. Adv. Energy Mater, 2016, 6(9): 1502423.
24. Guo D L, Hu C G, Xi Y, et al. Strain effects to optimize thermoelectric performance of doped Bi2O2Se via tran−blaha modified becke−johnson density functional theory. Journal of Physical Chemistry C, 2013, 117(41): 21597−21602.
25. Sun Y, Zhang C, Cao C, et al. Co−doping for significantly improved thermoelectric figure of merit in p−type Bi1−2xMgxPbxCuSeO oxyselenides. Ceramics International, 2017, 43(18): 17186−17193.
26. Hsiao C−L, Qi X. The oxidation states of elements in pure and Ca−doped BiCuSeO thermoelectric oxides. Acta Materialia, 2016, 102: 88−96.

Preprints (www.preprints.org) | NOT PEER-REVIEWED | Posted: 7 November 2023 doi:10.20944/preprints202311.0427.v1

27. Lei J, Guan W, Zhang D, et al. Isoelectronic indium doping for thermoelectric enhancements in BiCuSeO. Applied Surface Science, 2019, 473: 985–991.
28. Kim D H, Hong H Y, Lee J K, et al. Crystal structure and thermoelectric transport performance of Cu–deficient BiCuSeO oxyselenides. Journal of Materials Research and Technology, 2020, 9(6): 16202–16213.
29. Chen C, Delorme F, Schoenstein F, et al. Synthesis, sintering, and thermoelectric performance of Co1−xMxO (M = Na, 0 ≤ x ≤ 0.07; M = Ag, 0 ≤ x ≤ 0.05). Journal of the European Ceramic Society, 2019, 39(2–3): 346–351.
30. Zhang B, Rousse G, Foix D, et al. Microsized Sn as advanced anodes in glyme–based electrolyte for Na–Ion batteries. Adv Mater, 2016, 28(44): 9824–9830.
31. Li C, Guo D, Li K, et al. Remarkable enhancement in thermoelectric performance of BiCuSeO through biaxial strain modulation. Physica E: Low–dimensional Systems and Nanostructures, 2018, 97: 392–400.
32. Zhu H, Su T, Li H, et al. Thermoelectric performance of BiCuSeO doped with Pb. Solid State Communications, 2018, 278: 1–5.

Disclaimer/Publisher's Note: The statements, opinions and data contained in all publications are solely those of the individual author(s) and contributor(s) and not of MDPI and/or the editor(s). MDPI and/or the editor(s) disclaim responsibility for any injury to people or property resulting from any ideas, methods, instructions or products referred to in the content.